Int. J. Bio-Inorg. Hybr. Nanomater., 10(1): 27-41, Spring 2021

Theoretical investigation of encapsulation of the two azomethine derivatives into BN(6,6-8) nanotube: a DFT study

S. Esmaeili[1], M. Khaleghian[2], M. Samadizadeh[3]*

[1,3] *Department of Chemistry, Central Tehran Branch, Islamic Azad University, Tehran, Iran*
[2] *Department of Chemistry, Islamshahr Branch, Islamic Azad University, Islamshahr, Iran*

Received: 6 October 2020; Accepted: 8 December 2020

ABSTRACT: The purpose of this study is a better understanding of the encapsulation and interaction two azomethines (FUR and TIO) into BN nanotube [BNNT(6,6-8)]. The electronic and adsorption properties of the molecules FUR and TIO over the BNNT were theoretically investigated in the solvent water with the B3LYP/6-31G* level of theory. With the non-bonded interaction of two azomethines, the electronic properties of the BN nanotube can be significantly changed. The electronic spectra of the molecules FUR, TIO and complexes FUR/BNNT and TIO/BNNT were calculated by TD-DFT method for the study of adsorption effects. According to the NBO results, the molecules FUR, TIO and BNNT(6,6-8) play as both electron donor and acceptor at the complexes FUR/BNNT and TIO/BNNT. On the other hand, the charge transfer is occurred between the bonding, antibonding or nonbonding orbitals in the molecules azomethine and BNNT(6,6-8). As a consequence, BNNT(6,6-8) can be considered as a delivery or absorbent system.

Keywords: *Azomethine, BNNT(6,6-8), Encapsulation, NBO analysis, TD-DFT*

INTRODUCTION

The carbon nanotubes are as one of the attractive materials in which are used in field of physic, biotechnology, biomedicine and bio-chemistry due to their unique mechanical and electronic properties [1]. Boron nitride nanostructure has the band gap energy of about 6 eV [2]. Different electronic, optical and magnetic properties are expected to be revealed [3]. Therefore, many studies on Boron nitride nanomaterials such as Boron nitride nanotubes [3,4], Boron nitride nanocapsules [3], Boron nitride clusters [3,5] and Boron nitride nanoparticles [6,7] have been reported. It is expected that these compounds are useful for the electronics, semiconductor with high thermal stability and nanowires [8]. The Boron Nitride Nanotubes (BNNTs) have a band gap of about 5.5 eV [9]. Azomethines are one of the largest and most diverse combinations of synthetic organic dyes are being used today [10]. Azo compounds are extremely important and are moderately strong and chemically stable and colorants and broadly utilized substances in the textile, paper, coloring agents for foods and cosmetics industries [11,12]. Azo groups were reported to establish a variety of biological activities containing antibacterial, antifungal, pesticidal, antiviral

(*) Corresponding Author - e-mail: mehr.khaleghian97@gmail.com

and anti-inflammatory activities [13,14]. Azomethines are also used in photoluminescence materials [15], optical materials and devices [14], organic light-emitting diodes [16], photovoltaic cells [17] and polarizing films [13,14]. Density functional theory (DFT) studies provide more useful information on the interaction between nanotubes and delivered drug molecules. The adsorption and interaction of anticancer drugs such as cisplatin [18], carboplatin [19], paclitaxel [20], methotrexate [21] and doxorubicin [22] with BN nanotubs have already been studied. DFT studies can provide more useful information on the interaction between nanotubes with various compounds such as drugs and dye molecules [23-26]. Sheikhi and co-workers [2] have investigated interaction between a new azomethine derivative and BN(6,6-7) Nanotube by DFT calculations. They are discussed on electronic properties, chemical shift tensors, electronic spectra natural charge of the azomethine and BN(6,6-7) Nanotube in the complex BN(6,6-7)/azomethine. In the current study, our purpose is to understand the ability of BN nanotube for the encapsulation of the two azomethines (0E,4E)-4-(2-phenyldiazenyl)-N-(2-furfurylidene) benzenamine (FUR (0E,4E)-4-(2-phenyldiazenyl)-N-(2-thiophenylidene)benzenamine (TIO) [27] based on DFT calculations. We have studied thermodynamic parameters, frontier molecular orbitals (FMO), quantum molecular descriptors, natural bond orbitals (NBO), and absorption spectrum of the molecule FUR, TIO, BNNT(6,6-8) and complexes FUR/BNNT and TIO/BNNT.

COMPUTATIONAL METHODS

In the current study, the interaction and encapsulation between two azomethines including FUR and TIO with the BNNT(6,6-8) are taken into consideration. The Polarized Continuum Model (PCM) [10] was used for the calculations of solvent effect. The quantum chemical calculations have been performed using the density functional theory (DFT) calculations at the B3LYP/6-31G* level of theory by the Gaussian 09W program [28] for optimization of the molecule FUR, TIO, BNNT(6,6-8), and complexes FUR/BNNT and TIO/BNNT. We have defined the adsorption energies (E_{ad}) [2] of FUR and TIO over BN nanotube that is determined by using the following equations:

$$E_{ad} = E_{FUR/BNNT} - [E_{FUR} + E_{BNNT}] \quad (1)$$

$$E_{ad} = E_{TIO/BNNT} - [E_{TIO} + E_{BNNT}] \quad (2)$$

Where, $E_{FUR/BNNT}$ and $E_{TIO/BNNT}$ are the adsorption energies of the molecules FUR and TIO on the BNNT nanotube, respectively. Also, E_{FUR}, E_{TIO} and E_{BNNT} are energies of the molecules FUR, TIO and BN nanotube, respectively.

Natural bond orbital (NBO) [8], density of states (DOS), and frontier molecular orbitals (FMO) analysis [29] were performed by using B3LYP method and 6-31G* basis set. The thermodynamic parameters, molecular orbital (MO) calculations of the investigated compounds such as E_{HOMO}, E_{LUMO}, energy gap between LUMO and HOMO were performed. The optimized molecular structures, DOS plots and the orbital's graphs were visualized by and Gauss view [30] and GaussSum [31] programs. Time Dependent Density Functional Theory (TD-DFT) method [32] was used for the calculation of electronic transitions of the molecules FUR, TIO and the complexes FUR/BNNT and TIO/BNNT.

RESULTS AND DISCISSION

Optimized Structures

At first, we optimized the structures of the molecules FUR, TIO, BN nanotube and the complexes FUR/BNNT and TIO/BNNT using B3LYP/6-31G* level of theory in a solvent water. The optimized structures are shown in Figs. 1,2.

Table 1 shows the thermochemical parameters such as the sum of electronic and thermal energies (E+T), sum of electronic and thermal enthalpies (E+H), sum of electronic and thermal free energies (E+G), and entropy (S) of the molecules FUR, TIO, BNNT(6,6-8) and complexes FUR/BNNT and TIO/BNNT optimized using B3LYP/6-31G* level of theory. According to the summarized results in Table 1, with the interaction of the molecules FUR and TIO with BNNT(6,6-8), the thermal, gibbs and enthalpy energies values decrease.

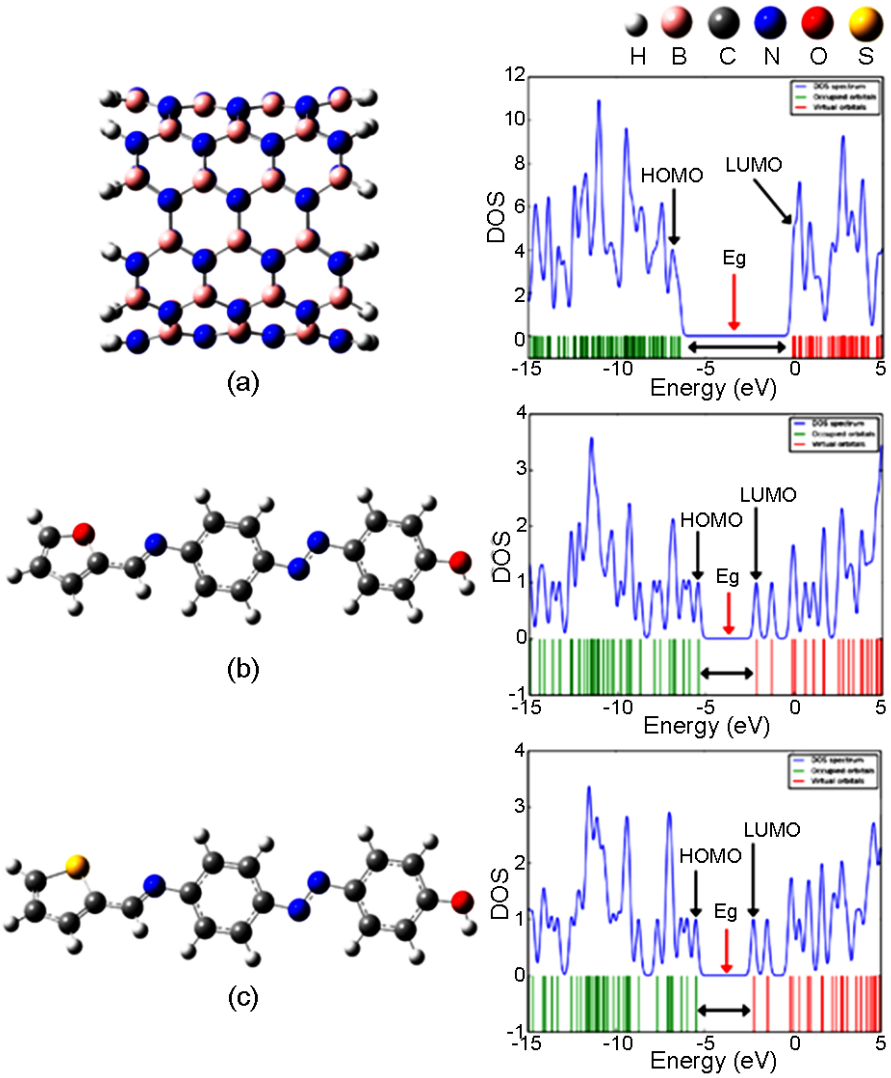

Fig. 1. The optimized geometry of the BN nanotube (a), FUR (b), TIO (c) and DOS plots using B3LYP/6-31G* level of theory.

Energy values reflect the reduced reactivity and increasing the stability of the molecules FUR and TIO in non-bonded interaction with BNNT(6,6-8). The calculated energies for the complex TIO/BNNT are the most negative rather than the complex FUR/BNNT, therefore the complex TIO/BNNT has the most stability comparing with the complex FUR/BNNT.

Electronic Properties

The frontier molecular orbitals including HOMO and LUMO are indicated as important parameters in the chemical reactions [32]. The HOMO and LUMO energies show the ability to donate an electron and obtain an electron respectively [10]. The molecular orbitals have a important role in charge transfer phenomenon in molecular systems [10]. The energy gap between HOMO and LUMO orbitals ($Eg = E_{LUMO} - E_{HOMO}$) is an significant factor in determining electrical transport properties in molecules [8]. We have studied the intermolecular interaction effects between the molecules FUR, TIO with BNNT(6,6-8) on the electronic properties. The computed results are listed in Table 2.

The adsorption energies (E_{ad}) of the molecules FUR and TIO over the BNNT(6,6-8) are computed about 0.65 eV and 0.70 eV, respectively, therefore, the interaction of the FUR and TIO with the BNNT(6,6-8) is endothermic (Table 2). It is indicated a strong chemisorption in the complex FUR/BNNT comparing with TIO/BNNT. After the adsorption of molecule FUR toward BNNT(6,6-8), the energy of HOMO is

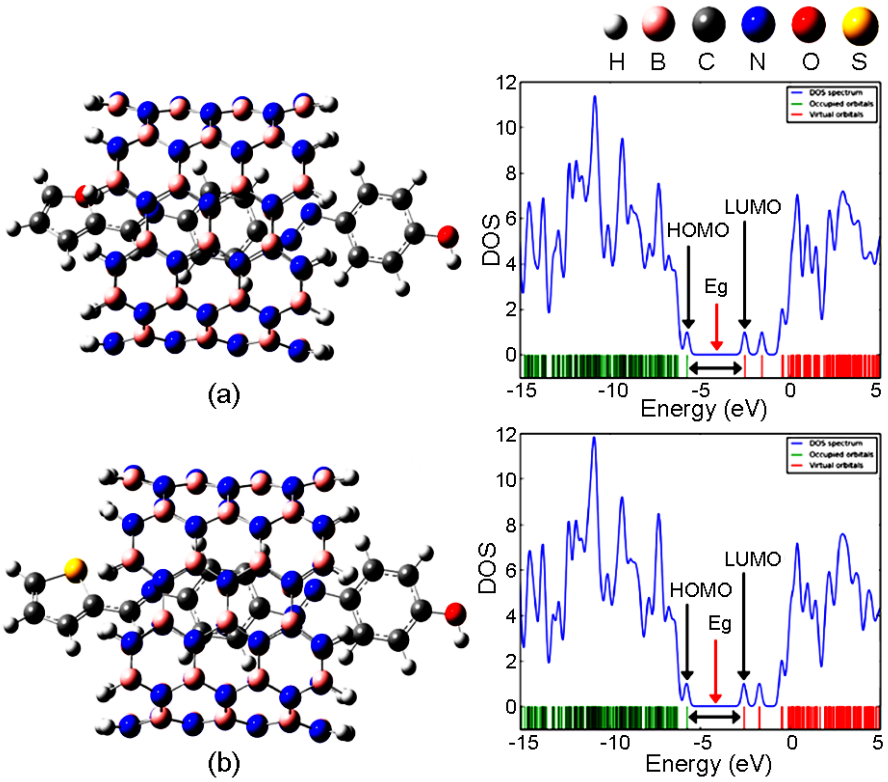

Fig. 1. The optimized geometry of the complexes FUR/BNNT (a), TIO/BNNT (b) and DOS plots using B3LYP/6-31G* level of theory.

increased from -6.47 in BN nanotube to -5.71, while the energy of LUMO is decreased from -0.07 eV to -2.51 eV in the complex FUR/BNNT. The energy of HOMO is increased from -6.47 eV in BN nano ring to –5.74 eV in the complex TIO/BNNT, whereas the energy of LUMO is decreased from -0.07 eV to -2.56 eV. The frontier orbitals graphs of the molecules FUR, TIO, BNNT(6,6-8), FUR/BNNT and TIO/BNNT is displayed in Fig. 3. As shown in Fig. 3, the electron density of HOMO orbital in the BNNT(6,6-8) is mainly situated on nitrogen atoms, whereas the LUMO orbital is localized on boron atoms. The electron density of HOMO and LUMO orbitals in the molecule FUR is mainly localized on the whole molecule, whereas the electron density of HOMO orbital in the molecule TIO is mainly localized on thiophene ring and the electron density of LUMO orbital is mainly localized on the whole molecule. The HOMO and LUMO orbitals of the complexes FUR/BNNT and TIO/BNNT focus only on the molecule FUR and TIO.

The energy gap values of the title molecules and complexes are reported in Table 2. Calculated DOS plots [8] in Fig. 1,2 also display the energy gaps of the investigated structures. As can be seen from Table 2, the energy gaps are decreased from 6.40 eV in BNNT(6,6-8) to 3.20 and 3.18 eV in the complexes FUR/BNNT and TIO/BNNT, respectively. These results show a basic increasing in electrical conductivity

Table 1. The thermochemical parameters of the molecules FUR, TIO, BNNT(6,6-8), and complexes FUR/BNNT and TIO/BNNT calculated by B3LYP/6-31G* level of theory.

Parameters	FURFU	TIO	BNNT	FUR/BNNT	TIO/BNNT
E+G (Hartree)	-970.039	-1293.026	-3361.804	-4331.793	-4654.776
E+H (Hartree)	-969.972	-1292.957	-3361.678	-4331.624	-4654.607
E+T (Hartree)	-969.973	-1292.958	-3361.679	-4331.625	-4654.608
S (cal/mol.K)	142.407	145.239	265.155	356.339	356.110

Table 2. The computed electronic properties of the molecules FUR, TIO, BNNT(6,6-8) and the complexes FUR/BNNT and TIO/BNNT at the B3LYP/6-31G* level of theory in the solvent water.

Property	FUR	TIO	BNNT	FUR/BNNT	TIO/BNNT
Dipole moment (Debye)	3.354	3.113	0.000	2.726	2.671
E(Hartree)	-970.258	-1293.241	-3362.454	-4332.688	-4655.669
E_{HOMO} (eV)	-5.43	-5.47	-6.47	-5.71	-5.74
E_{LUMO} (eV)	-2.13	-2.21	-0.07	-2.51	-2.56
Eg (eV)	3.30	3.26	6.40	3.20	3.18
E_{ads} (eV)	-	-	-	0.65	0.70
I (eV)	5.43	5.47	6.47	5.71	5.74
A (eV)	2.13	2.21	0.07	2.51	2.56
χ (eV)	3.78	3.84	3.27	4.11	4.15
η (eV)	1.65	1.63	3.20	1.60	1.59
μ (eV)	-3.78	-3.84	-3.27	-4.11	-4.15
ω (eV)	4.33	4.52	3.34	5.28	5.41
S (eV)	0.303	0.306	0.312	0.312	0.314

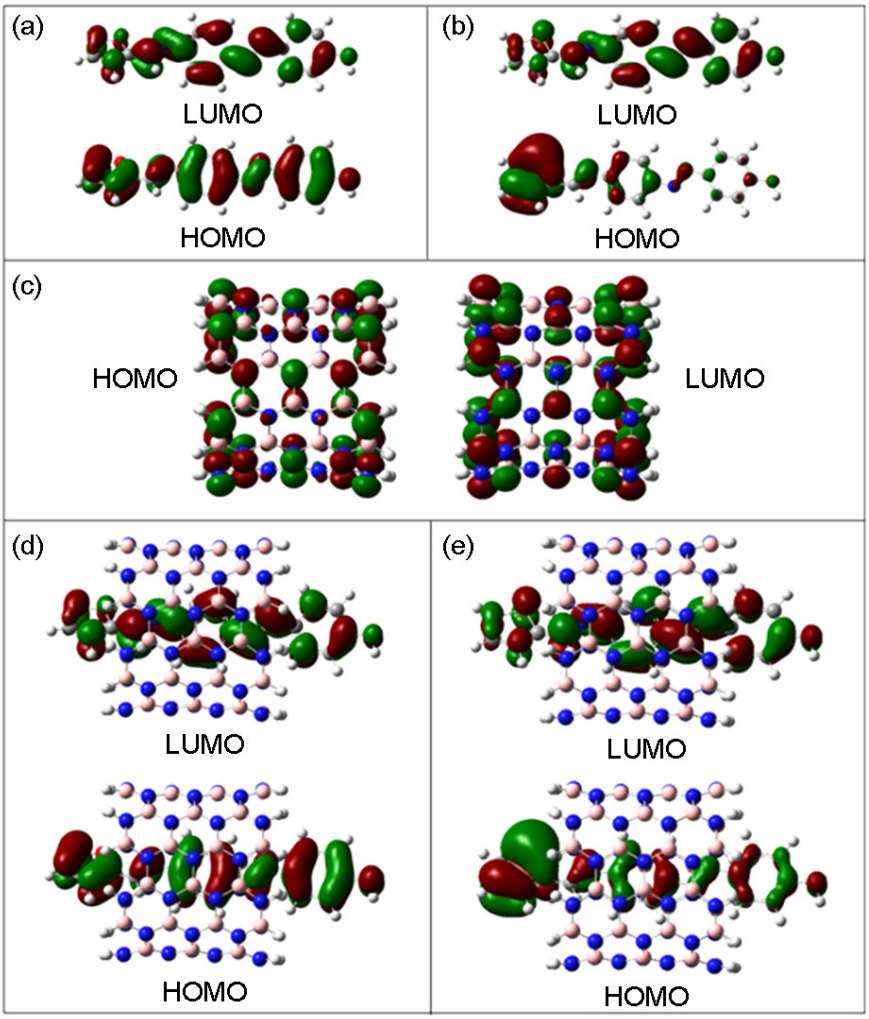

Fig. 3. The calculated HOMO, LUMO orbitals the molecules FUR, TIO, BNNT(6,6-8) and the complexes FUR/BNNT and TIO/BNNT at the B3LYP/6-31G* level of theory.

of the complexes rather than the isolated BNNT(6,6-8). According to the results, we believe that the encapsulation of TIO into BNNT(6,6-8) is better due to the lower energy gap (3.26 eV) rather than the molecule FUR (3.30 eV). The quantum molecular descriptors for the title systems such as ionization potential (I), electron affinity (A), global hardness (η), electronegativity (χ), electronic chemical potential (μ), electrophilicity (ω) and chemical softness (S) are computed according to follows equations, respectively [8]:

$$I=-E_{HOMO} \quad (3)$$

$$A=-E_{LUMO} \quad (4)$$

$$\eta=I-A/2 \quad (5)$$

$$\chi=I+A/2 \quad (6)$$

$$\mu=-(I+A)/2 \quad (7)$$

$$\omega=\mu^2/2\eta \quad (8)$$

$$S=1/2\eta \quad (9)$$

That is reported in Table 2. The stability of the molecules is related to hardness which is a tool to understand chemical reactivity [1]. As shown in Table 2, the values of global hardness (η) for BNNT are 3.20 eV and after capsulation of FUR and TIO into BNNT are changed to 1.60 and 1.59 eV in the complexes FUR/BNNT and TIO/BNNT, respectively. This result indicates that the η value of BNNT(6,6-8) decrease with the interaction of FUR and TIO with BN nanotube and the complex FUR/BNNT (1.60 eV) is harder than the TIO/BNNT (1.59 eV). The reactivity of TIO is higher due to the lower η value (1.63 eV) compared with FUR (1.65 eV). The electronic chemical potential (μ) of the complexes FUR/BNNT and TIO/BNNT also decreased. Therefore, the complexes have a high chemical activity, low chemical stability and they are the soft systems rather than two azomethine and BNNT(6,6-8). The dipole moment value of BNNT(6,6-8) is increased by encapsulation of the molecules FUR and TIO from 0.000 to 2.726 and 2.671 Debye in complexes FUR/BNNT and TIO/BNNT, respectively (see Table 2). The change of dipole moment after encapsulation of two azomethine into BNNT(6,6-8) indicates a charge transfer between two azomethine and BN nanotube.

NBO analysis

NBO analysis is an important method for studying intra- and inter-molecular bonding and interaction between bonds in molecular systems [32]. The electron delocalization from donor orbitals to acceptor orbitals describes a conjugative electron transfer process between them [33]. For each donor orbital (i) and acceptor orbital (j), the stabilization energy $E^{(2)}$ associated with the delocalization i→j is calculated [32]:

$$E^{(2)} = \Delta E_{ij} = q_i \frac{F(i,j)^2}{\varepsilon_j - \varepsilon_i} \quad (10)$$

The stabilization energy ($E^{(2)}$) describes the amount of the participation of electrons in the resonance between atoms of the molecules [8]. The high $E^{(2)}$, the more donation tendency from electron donor orbitals to electron acceptor orbitals [32]. The NBO analysis for complexes FUR/BNNT and TIO/BNNT have been

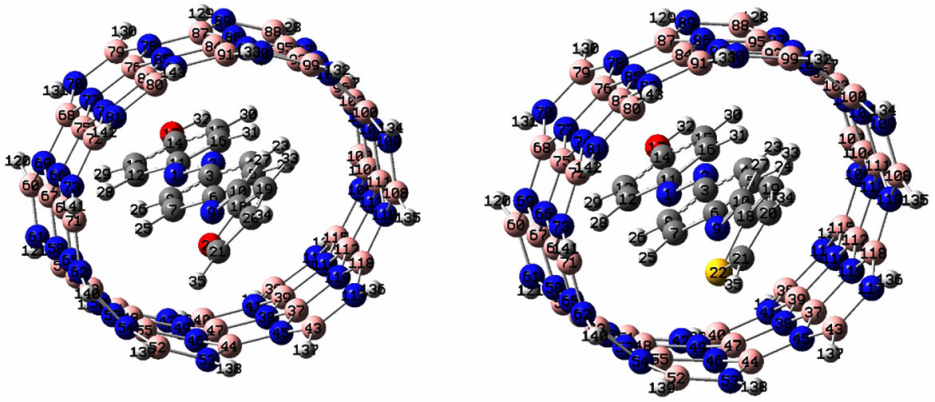

(a) (b)

Fig. 4. The optimized structures of the complexes FUR/BNNT and TIO/BNNT at the B3LYP/6-31G* level of theory with atom numbering.

performed by B3LYP/6-31G* level of theory and the results are reported in Table 3 (Atoms numbering is according to Fig. 4).

According to the results of NBO analysis, the π→π* transitions from FUR to BNNT(6,6-8) occur as π(N1-N2)→π*(B36-N116),π(N1-N2)→π*(N70-B79), π(N1-N2)→π*(N78-B87) with stabilization energies ($E^{(2)}$) about 0.11, 0.13, 0.06 kcal/mol respectively. It is observed that π(N1-N2)→π*(N70-B79) interaction has the highest resonance energy (0.13 kcal/mol) rather than other π→π* transitions. The σ→π* transitions from FUR to BNNT(6,6-8) also take place

Table 3. The donor-acceptor interactions and second-order perturbation energies ($E^{(2)}$, kcal/mol) related to charge transfer between FUR and BNNT(6,6-8) in complex FUR/BNNT calculated using the B3LYP/6-31G* method.

Donor (i)	Acceptor (j)	$E^{(2)a}$ (kcal/mol)	E(j)-E(i)[b] (a.u.)	F(i , j)[c] (a.u.)
π(N1-N2)	π*(B36-N116)	0.11	0.43	0.006
	π*(N70-B79)	0.13	0.43	0.007
	π*(N78-B87)	0.06	0.44	0.005
σ(C4-H23)	π*(N86-B95)	0.94	0.60	0.022
	π*(N94-B103)	0.43	0.60	0.015
	π*(B96-N97)	0.82	0.60	0.021
	π*(B104-N105)	1.42	0.60	0.028
σ(C5-H24)	π*(N94-B103)	0.61	0.61	0.018
	π*(N102-B111)	1.01	0.61	0.023
σ(C7-H25)	π*(B56-N65)	2.98	0.59	0.040
σ(C8-H26)	π*(N50-B59)	0.93	0.60	0.022
	π*(N58-B67)	0.66	0.60	0.019
σ(C10-H27)	π*(N90-B91)	0.34	0.62	0.014
	π*(B100-N101)	0.13	0.62	0.009
n1(N1)	π*(N42-B51)	0.12	0.47	0.007
	π*(B60-N61)	0.12	0.47	0.007
	π*(B68-N69)	0.07	0.48	0.006
n1(N2)	π* (N78-B87)	0.08	0.48	0.006
	π*(B88-N89)	0.12	0.47	0.007
	π*(N106-B115)	0.08	0.48	0.006
n1(N9)	π*(B44-N45)	0.38	0.42	0.012
	π*(N54-B63)	0.26	0.43	0.010
n1(O22)	π*(B52-N53)	0.55	0.66	0.017
	π*(N62-B71)	0.06	0.66	0.006
n2(O22)	π*(N62-N71)	0.09	0.42	0.006
π(N50-B59)	σ*(C8-H26)	0.37	0.79	0.016
σ(B56-N58)	σ*(C7-H25)	0.07	1.20	0.008
σ(B56-N65)	σ*(C7-H25)	0.05	1.20	0.007
π(B56-N65)	σ*(C7-H25)	1.73	0.80	0.035
π(B58-N67)	σ*(C8-H26)	0.08	0.79	0.007
π(B60-N61)	σ*(C12-H28)	0.18	0.77	0.011
π(B60-N61)	σ*(C12-H28)	0.18	0.77	0.011
σ(B60-H120)	σ*(C12-H28)	0.11	0.89	0.009
σ(B63-N65)	σ*(C7-H25)	0.07	1.19	0.008
π(B64-N66)	σ*(C7-H25)	0.23	0.80	0.013
π(B96-N97)	σ*(C4-H23)	0.34	0.80	0.016
π(N98-B107)	σ*(C4-H23)	0.06	0.82	0.007
	σ*(C16-H31)	0.22	0.78	0.012
σ(B99-H132)	σ*(C19-H33)	0.25	0.89	0.013
π(B100-N101)	σ*(C10-H27)	0.09	0.72	0.008
π (N102-B111)	σ*(C5-H24)	0.85	0.78	0.024
	σ*(C10-H27)	0.06	0.72	0.006
π(B104-N105)	σ*(C4-H23)	1.35	0.81	0.031

[a] $E^{(2)}$ Energy of hyperconjucative interactions.

[b] Energy difference between donor and acceptor i and j NBO orbitals.

[c] F(i, j) Is the Fock matrix element between i and j NBO orbitals.

in complex FUR/BNNT and they have the higher resonance energies ($E^{(2)}$) rather than π→π* transition. The important σ→π* transitions are including σ(C4-H23)→π*(N86-B95),σ(C4-H23)→π*(B104-N105),σ(C5-H24)→π*(N102-B111),σ(C7-H25)→π*(B56-N65),σ(C8-H26)→π*(N50-B59) interactions with stabilization energies ($E^{(2)}$) of 0.94, 1.42, 1.01, 2.98, 0.93 kcal/mol, respectively. The important n→π* transitions are such as n1(N9)→π*(B44-N45),n1(N9)→π*(N54-B63), n1(O22)→π*(B52-N53) interactions with resonance energies ($E^{(2)}$) of 0.38, 0.26, 0.55 kcal/mol, respectively. The results of NBO analysis shows that π→σ* and σ→σ* transitions from BNNT(6,6-8) to

Table 4. The donor-acceptor interactions and second-order perturbation energies (E(2), kcal/mol) related to charge transfer between TIO and BNNT(6,6-8) in complex TIO/BNNT calculated using the B3LYP/6-31G* method.

Donor (i)	Acceptor (j)	$E^{(2)a}$ (kcal/mol)	E(j)-E(i)[b] (a.u.)	F(i , j)[c] (a.u.)
π(N1-N2)	π*(B40-N41)	0.09	0.44	0.006
	π*(B68-N69)	0.07	0.45	0.005
	π*(N78-B87)	0.11	0.44	0.006
σ(N1-N2)	π*(N86-B95)	0.75	0.60	0.020
	π*(N94-B103)	1.66	0.60	0.030
	π*(B104-N105)	1.22	0.60	0.026
σ(C7-H25)	π*(N46-B55)	1.04	0.60	0.024
	π*(B64-N66)	1.66	0.59	0.030
σ(C8-H26)	π*(N58-B67)	0.90	0.60	0.022
n1(N1)	π*(B40-N41)	0.10	0.48	0.006
	π*(N42-B51)	0.11	0.47	0.007
	π*(N50-B59)	0.12	0.48	0.007
	π*(B60-N61)	0.09	0.47	0.006
	π*(B68-N69)	0.16	0.49	0.008
n1(N2)	π*(N78-B87)	0.15	0.48	0.008
	π*(B96-N97)	0.13	0.48	0.007
	π*(N106-B115)	0.15	0.48	0.008
n1(N9)	π*(B44-N45)	0.29	0.42	0.010
	π*(B52-N53)	0.14	0.42	0.007
n1(S22)	π*(B52-N53)	0.36	0.72	0.015
	π*(N62-B71)	0.05	0.73	0.006
n2(S22)	π*(B43-N117)	0.08	0.32	0.005
	π*(N62-B71)	0.19	0.33	0.007
π(N50-B59)	σ*(C8-H26)	0.10	0.79	0.008
σ(B51-H122)	σ*(C12-H28)	0.10	0.90	0.009
π(B52-N53)	σ*(C21-S22)	0.08	0.50	0.006
π (N54-B63)	σ*(C7-H25)	0.10	0.80	0.009
π(B56-N65)	σ*(C7-H25)	1.21	0.80	0.030
π(N58-B67)	σ*(C8-H26)	0.58	0.79	0.020
σ(B59-N61)	σ*(C12-H28)	0.06	1.18	0.007
π(B60-N61)	σ*(C8-H26)	0.06	0.80	0.007
	σ*(C12-H28)	0.86	0.78	0.024
σ(B60-H120)	σ*(C12-H28)	0.15	0.90	0.011
π(N62-B71)	σ*(C7-H25)	0.06	0.81	0.007
π(N90-B91)	σ*(C10-H27)	0.08	0.72	0.007
π(N94-B103)	σ*(C4-H23)	0.17	0.81	0.011
π(N98-B107)	σ*(C16-H31)	0.55	0.79	0.019
σ(B99-H132)	σ*(C19-H33)	0.30	0.89	0.015
π(B100-N101)	σ*(C5-H24)	0.19	0.78	0.012
π(N102-B111)	σ*(C5-H24)	0.55	0.78	0.020
π(B104-N105)	σ*(C4-H23)	1.61	0.81	0.034

[a] $E^{(2)}$ Energy of hyperconjucative interactions.

[b] Energy difference between donor and acceptor i and j NBO orbitals.

[c] F(i, j) Is the Fock matrix element between i and j NBO orbitals.

FUR also occur in complex FUR/BNNT. Among the σ→σ* electron charge transfers are such as σ(B56-N58)→σ*(C7-H25),σ(B60-H120)→σ*(C12-H28), σ(B99-H132)→σ*(C19-H33) with stabilization energies ($E^{(2)}$) 0.07, 0.11 and 0.25 kcal/mol respectively. According to NBO analysis, the main π→σ* interactions are π(B56-N65)→σ*(C7-H25), π(N102-B111)→σ*(C5-H24),π(B104-N105)→σ*(C4-H23) transitions with resonance energies ($E^{(2)}$) about 1.73, 0.85, 1.35 kcal/mol, respectively. Thus, FUR and BNNT(6,6-8) acts as both electron donor and electron acceptor, therefore charge transfer take place between FUR and BNNT(6,6-8) in the complex FUR/BNNT.

The NBO analysis shows that π→π*, σ→π*, n→π* transitions from TIO to BNNT(6,6-8) take place in complex TIO/BNNT (Table 4). As shown in Table 4, the π→π* transitions from TIO to BNNT(6,6-8) take place as π(N1-N2)→π*(B40-N41), π(N1-N2)→π*(B68-N69), π(N1-N2)→π*(N78-B87) interactions with resonance energies ($E^{(2)}$) about 0.09, 0.07 and 0.11 kcal/mol, respectively. The σ→π* transitions from TIO to BNNT(6,6-8) are such as σ(N1-N2)→π*(N86-B95),σ(N1-N2)→π*(N94-B103), σ(N1-N2)→π*(B104-N105),σ(C7-H25)→π*(N46-B55), σ(C7-H25)→π*(B64-N66), σ(C8-H26)→π*(N58-B67) interactions with stabilization energies ($E^{(2)}$) about 0.75, 1.66, 1.22, 1.04, 1.66 and 0.90 kcal/mol, respectively. The σ(N1-N2)→π*(N94-B103) and σ(C7-H25)→π*(B64-N66) interactions have the higher resonance energy (1.66 kcal/mol) rather than the other σ→π* transitions. The important n→π* transitions in the complex TIO/BNNT is observed for n1(N9)→π*(B44-N45) and n1(S22)→π*(B52-N53) interactions with stabilization energies ($E^{(2)}$) about 0.29 and 0.36 kcal/mol, respectively. Also, the π→σ* and σ→σ* transitions from BNNT(6,6-8) to TIO occur in complex TIO/BNNT. According to results of NBO analysis, the important σ→σ* interaction from BNNT(6,6-8) to TIO is such as σ*(B99-H132)→σ*(C19-H33) transition with resonance energy ($E^{(2)}$) of 0.30 kcal/mol. According to NBO analysis, the important π→σ* interactions from BNNT(6,6-8) to TIO are including π(B56-N65)→σ*(C7-H25),π(B60-N61)→σ*(C12-H28), π(B104-N105)→σ*(C4-H23) transitions with resonance energies ($E^{(2)}$) about 1.21, 0.86, 1.61 kcal/mol, respectively. Thus, TIO and BNNT(6,6-8) acts as both electron donor and electron acceptor in the complex TIO/BNNT and therefore charge transfer take place between TIO and BNNT(6,6-8).

Table 5. Electronic absorption spectrum of the molecule FUR and complex FUR/BNNT calculated by TDB3LYP/6-31G* method

FUR				
Excited State	Wavelength (nm)	Excitation Energy (eV)	Configurations Composition (corresponding transition orbitals)	Oscillator Strength (f)
$S_0 \rightarrow S_1$	481	2.57	H-1→L (90%), H-1→L+1 (9%)	0.00
$S_0 \rightarrow S_2$	407	3.04	H→L (98%)	1.42
$S_0 \rightarrow S_3$	338	3.66	H-2→L (32%), H→L+1 (60%), H-3→L (3%), H-3→L+1 (2%)	0.05
$S_0 \rightarrow S_4$	316	3.91	H-3→L (39%), H-2→L (40%), H-6→L (4%), H-6→L+1 (3%), H-3→L+1 (4%), H→L+1 (6%)	0.01
$S_0 \rightarrow S_5$	308	4.02	H-1→L+1 (86%) H-1→L (9%)	0.00
$S_0 \rightarrow S_6$	307	4.03	H-4→L (70%), H-3→L (7%), H-2→L (6%), H-1→L+1 (2%), H→L+1 (4%), H→L+3 (8%)	0.00
$S_0 \rightarrow S_7$	299	4.13	H-4→L (17%), H-3→L (31%), H-2→L (18%), H→L+1 (23%), H-6→L (3%), H-2→L+1 (4%)	0.01
$S_0 \rightarrow S_8$	292	4.24	H-5→L (82%), H→L+2 (11%), H-5→L+1 (3%)	0.00
$S_0 \rightarrow S_9$	262	4.72	H-6→L (35%), H-3→L+1 (33%), H-6→L+1 (5%), H-3→L (6%), H-2→L+1 (9%), H→L+1 (3%)	0.17
$S_0 \rightarrow S_{10}$	260	4.75	H-3→L+1 (13%), H-2→L+1 (75%), H-3→L (4%), H→L+4 (3%)	0.12
$S_0 \rightarrow S_{11}$	253	4.89	H-6→L (14%), H-4→L+1 (57%), H-3→L+1 (16%), H→L+2 (5%), H→L+3 (3%)	0.02

$S_0 \rightarrow S_{12}$	252	4.90	H-5→L (11%), H-4→L+1 (12%), H→L+2 (59%), H-6→L (2%), H-5→L+1 (4%), H-1→L+2 (8%)	0.03
$S_0 \rightarrow S_{13}$	251	4.92	H-1→L+2 (92%) H→L+2 (5%)	0.00
$S_0 \rightarrow S_{14}$	248	4.98	H-6→L (27%), H-4→L+1 (27%), H-3→L+1 (20%), H-2→L+1 (5%), H→L+1 (2%), H→L+2 (5%), H→L+3 (4%), H→L+4 (3%)	0.05
$S_0 \rightarrow S_{15}$	245	5.05	H→L+3 (71%), H-6→L (4%), H-4→L (6%), H-1→L+3 (9%)	0.06
$S_0 \rightarrow S_{16}$	243	5.08	H-1→L+3 (91%) H→L+3 (7%)	0.00
$S_0 \rightarrow S_{17}$	231	5.36	H-7→L (83%), H-5→L+1 (7%)	0.02
$S_0 \rightarrow S_{18}$	230	5.38	H-5→L+1 (71%) H-7→L (8%), H-2→L+2 (8%), H→L+2 (8%)	0.00
$S_0 \rightarrow S_{19}$	219	5.65	H-6→L+1 (68%) H-6→L (4%), H-3→L+1 (4%), H-2→L+2 (5%), H→L+4 (8%), H→L+5 (3%)	0.00
$S_0 \rightarrow S_{20}$	217	5.69	H-1→L+4 (84%), H-1→L+5 (10%), H-6→L+1 (2%)	0.00

FUR/BNNT

Excited State	Wavelength (nm)	Excitation Energy (eV)	Configurations Composition (corresponding transition orbitals)	Oscillator Strength (f)
$S_0 \rightarrow S_1$	514	2.41	H-1→L (78%), H-3→L (9%), H-2→L (4%), H-1→L+1 (7%)	0.00
$S_0 \rightarrow S_2$	420	2.94	H→L (97%)	0.84
$S_0 \rightarrow S_3$	395	3.13	H-3→L (12%), H-2→L (86%)	0.00
$S_0 \rightarrow S_4$	391	3.16	H-3→L (76%), H-1→L (14%), H-2→L (9%)	0.00
$S_0 \rightarrow S_5$	368	3.36	H-4→L (92%), H-6→L (6%)	0.02
$S_0 \rightarrow S_6$	358	3.45	H-5→L (97%)	0.00
$S_0 \rightarrow S_7$	346	3.57	H-7→L (95%), H-8→L (2%)	0.00
$S_0 \rightarrow S_8$	345	3.59	H-8→L (94%)	0.00
$S_0 \rightarrow S_9$	341	3.62	H-10→L (17%), H-9→L (14%), H-6→L (24%), H→L+1 (31%), H-10→L+1 (2%)	0.02
$S_0 \rightarrow S_{10}$	339	3.65	H-9→L (68%), H-6→L (21%), H→L+1 (6%)	0.00
$S_0 \rightarrow S_{11}$	334	3.70	H-10→L (38%), H-9→L (15%), H-6→L (22%), H-13→L (2%), H-12→L (3%), H-11→L (4%), H-10→L+1 (2%)	0.01
$S_0 \rightarrow S_{12}$	319	3.88	H-13→L (13%), H-11→L (24%), H-1→L+1 (37%), H-14→L (4%), H-10→L (7%), H-3→L+1 (3%), H-1→L (3%), H→L+2 (2%)	0.00
$S_0 \rightarrow S_{13}$	318	3.89	H-13→L (11%), H-11→L (15%), H-1→L+1 (43%), H-14→L (6%), H-12→L (2%), H-10→L (7%), H-3→L+1 (2%), H-1→L (3%), H→L+2 (2%)	0.00
$S_0 \rightarrow S_{14}$	312	3.96	H-13→L (26%), H-12→L (35%), H-11→L (33%), H-10→L (3%)	0.00
$S_0 \rightarrow S_{15}$	311	3.97	H-13→L (14%), H-12→L (49%), H-11→L (18%), H-10→L (10%) H→L+1 (2%)	0.00
$S_0 \rightarrow S_{16}$	310	3.99	H-6→L (20%), H→L+1 (52%), H-13→L (7%), H-12→L (5%), H-10→L (5%), H-4→L (2%)	0.00
$S_0 \rightarrow S_{17}$	305	4.05	H-14→L (80%), H-13→L (12%)	0.00
$S_0 \rightarrow S_{18}$	301	4.11	H-3→L+1 (34%), H-2→L+1 (47%), H-1→L+1 (8%)	0.00
$S_0 \rightarrow S_{19}$	300	4.13	H-15→L (84%), H-17→L (5%)	0.00
$S_0 \rightarrow S_{20}$	299	4.14	H-19→L (37%), H-16→L (34%), H-2→L+1 (13%), H-3→L+1 (3%), H→L+3 (3%)	0.00

*H-HOMO, L-LUMO

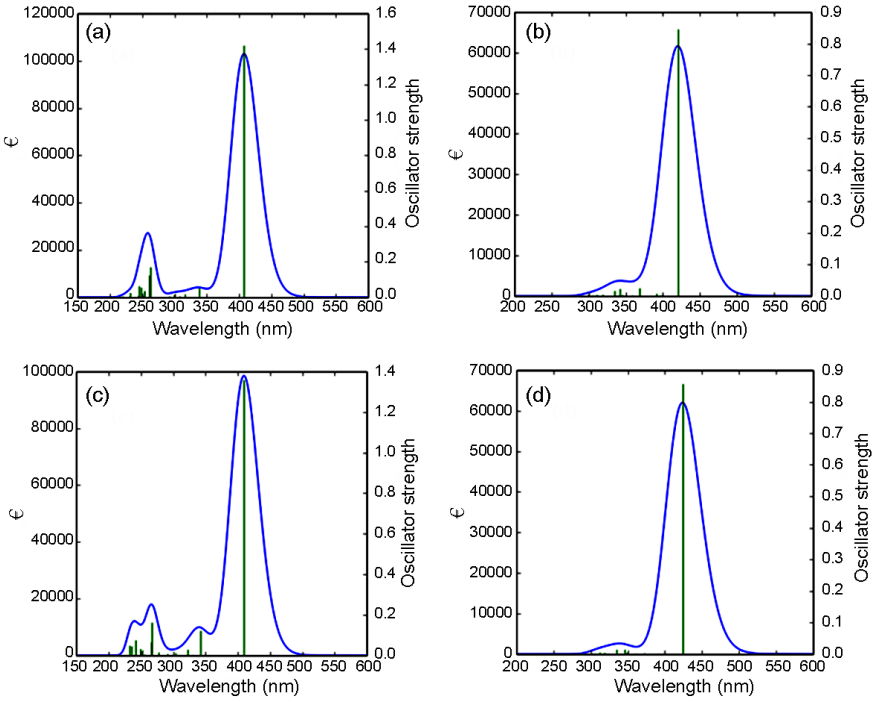

Fig. 5. UV spectrum of the FUR (a), complex FUR/BNNT (b), TIO (c), complex TIO/BNNT calculated by TDB3LYP/6-31G* method.

Electronic Structure and Excited States

In order to investigation of the encapsulation effect of FUR and TIO into BNNT(6,6-8) on the λ_{max}, we have computed the UV/Vis spectra of the molecules FUR, TIO and the complexes FUR/BNNT and TIO/BNNT using TD-DFT calculations at B3LYP/6-31G* method with considering 20 excited states which is reported in Tables 5,6. These tables indicate the λ_{max}, oscillator strength (f), and excitation energies (E).

The analysis of the calculated UV spectrum for the FUR exhibits λ_{max} at 407 nm (f = 1.42) (see Table 5). The charge transfer at λ_{max} = 407 nm is related to the excited state $S_0 \rightarrow S_2$ with one electron configuration such as H→L (98%). The other excited states of FUR have very small intensity and do not play any role in the formation of electron spectrum of the title compound (Table 5). The computed electronic absorption spectrum of FUR in the solvent water is shown in Fig. 5(a). The calculated value of λ_{max} is in good agreement with the experimental values [27]. With the encapsulation of FUR into the BNNT(6,6-8), λ_{max} is observed at 420 nm (f = 0.84). The charge transfer at λ_{max} = 420 is related to the excited state $S_0 \rightarrow S_2$ and is defined by eight configurations including H→L (97%) (Table 5). The other excited states of the complex FUR/BNNT have very small intensity and do not play any role in the formation of electron spectrum of this molecular system (Table 5). The theoretical electronic absorption spectrum of FUR/BNNT is observed in Fig. 5(b).

According to the theoretical UV spectrum of the FUR, λ_{max} is observed at 409 nm (f = 1.36) (Table 6). The charge transfer at λ_{max} = 409 nm is related to the excited state $S_0 \rightarrow S_2$ with one electron configurations such as H→L (96%). The calculated value of λ_{max} is in good agreement with the experimental values [27]. After the encapsulation of TIO into the BNNT(6,6-8), λ_{max} appear at 423 nm (f = 0.85). The charge transfer at λ_{max} = 423 is related to the excited state S0→S2 and is defined by one configuration including H→L (98%) (Table 6). The other excited states of FUR and complex TIO/BNNT have very small intensity and do not play any role in the formation of electron spectrum of the title compound (Table 6). The theoretical electronic absorption spectra of FUR and complex TIO/BNNT in the solvent water are shown in Fig. 5(c),(d). Thus, we found that encapsulation of the molecules FUR and TIO into the BNNT(6,6-8) enhances the value of λ_{max} and it can be considered as a bathochromic shift.

Table 6. Electronic absorption spectrum of TIO and complex TIO/BNNT calculated by TDB3LYP/6-31G* method.

TIO				
Excited State	Wavelength (nm)	Excitation Energy (eV)	Configurations Composition (corresponding transition orbitals)	Oscillator Strength (f)
$S_0 \rightarrow S_1$	513	2.41	H-1→L (88%), H-1→L+1 (12%)	0.00
$S_0 \rightarrow S_2$	409	3.02	H→L (96%)	1.36
$S_0 \rightarrow S_3$	341	3.62	H-2→L (22%), H→L+1 (66%), H-3→L (7%), H-3→L+1 (3%)	0.12
$S_0 \rightarrow S_4$	329	3.76	H-1→L (12%), H-1→L+1 (86%)	0.00
$S_0 \rightarrow S_5$	322	3.83	H-3→L (48%), H-2→L (37%), H-7→L (4%), H-3→L+1 (4%)	0.02
$S_0 \rightarrow S_6$	307	4.03	H-4→L (21%), H-3→L (24%), H-2→L (28%), H→L+1 (19%), H→L+3 (3%)	0.00
$S_0 \rightarrow S_7$	304	4.07	H-4→L (68%), H-3→L (6%), H-2→L (8%), H→L+1 (8%), H→L+3 (5%)	0.01
$S_0 \rightarrow S_8$	291	4.25	H-5→L (82%), H-5→L+1 (4%), H→L+2 (9%)	0.00
$S_0 \rightarrow S_9$	277	4.46	H-6→L (89%), H-2→L+1 (6%)	0.01
$S_0 \rightarrow S_{10}$	267	4.64	H-7→L (19%), H-3→L+1 (48%), H-2→L+1 (16%), H-7→L+1 (3%), H-3→L (5%), H→L+1 (2%)	0.16
$S_0 \rightarrow S_{11}$	266	4.65	H-3→L+1 (20%), H-2→L+1 (66%), H-6→L (4%), H-3→L (3%)	0.06
$S_0 \rightarrow S_{12}$	256	4.84	H-1→L+2 (99%)	0.00
$S_0 \rightarrow S_{13}$	255	4.85	H-7→L (23%), H-4→L+1 (61%), H-3→L+1 (8%), H→L+4 (2%)	0.00
$S_0 \rightarrow S_{14}$	252	4.90	H-7→L (37%), H-4→L+1 (36%), H-3→L+1 (9%), H-2→L+1 (3%), H→L+2 (3%), H→L+4 (4%)	0.02
$S_0 \rightarrow S_{15}$	249	4.97	H-5→L (13%), H-5→L+1 (12%), H→L+2 (60%), H-1→L+3 (6%)	0.03
$S_0 \rightarrow S_{16}$	248	4.98	H-1→L+3 (93%) H→L+2 (4%)	0.00
$S_0 \rightarrow S_{17}$	241	5.13	H→L+3 (84%), H-4→L (7%), H-4→L+4 (3%)	0.07
$S_0 \rightarrow S_{18}$	235	5.26	H-6→L+1 (89%)	0.04
$S_0 \rightarrow S_{19}$	232	5.33	H-5→L+1 (74%), H→L+2 (18%), H-2→L+2 (3%)	0.04
$S_0 \rightarrow S_{20}$	226	5.46	H-1→L+4 (83%), H-1→L+5 (14%)	0.00
BNNT/TIO				
Excited State	Wavelength (nm)	Excitation Energy (eV)	Configurations Composition (corresponding transition orbitals)	Oscillator Strength (f)
$S_0 \rightarrow S_1$	511	2.42	H-1→L (75%), H-3→L (8%), H-2→L (7%), H-1→L+1 (8%)	0.00
$S_0 \rightarrow S_2$	423	2.92	H→L (98%)	0.85
$S_0 \rightarrow S_3$	397	3.12	H-3→L (20%), H-2→L (63%), H-1→L (16%)	0.00
$S_0 \rightarrow S_4$	391	3.16	H-3→L (70%), H-2→L (28%)	0.00
$S_0 \rightarrow S_5$	371	3.33	H-4→L (93%), H-6→L (6%)	0.00
$S_0 \rightarrow S_6$	360	3.44	H-5→L (97%)	0.00
$S_0 \rightarrow S_7$	348	3.55	H-7→L (73%), H-6→L (15%), H-9→L (2%), H-8→L (4%), H→L+1 (3%)	0.00
$S_0 \rightarrow S_8$	347	3.57	H-8→L (73%), H-7→L (13%), H-6→L (5%), H→L+1 (4%)	0.00
$S_0 \rightarrow S_9$	345	3.58	H-8→L (20%), H-6→L (21%), H→L+1 (31%), H-11→L (2%), H-10→L (7%), H-9→L (3%), H-7→L (9%)	0.01
$S_0 \rightarrow S_{10}$	341	3.62	H-9→L (92%), H-6→L (3%), H→L+1 (2%)	0.00
$S_0 \rightarrow S_{11}$	334	3.70	H-11→L (13%), H-10→L (42%), H-6→L (22%), H-27→L (2%), H-17→L (2%), H-10→L+1 (2%), H-7→L (2%)	0.01

$S_0 \rightarrow S_{12}$	323	3.83	H-1→L+1 (76%) H-3→L+1 (4%), H-2→L+1 (5%), H-1→L (7%)	0.00
$S_0 \rightarrow S_{13}$	319	3.87	H-14→L (12%), H-13→L (11%), H-11→L (53%), H→L+1 (10%), H-6→L (5%), H→L+2 (4%)	0.00
$S_0 \rightarrow S_{14}$	317	3.90	H-10→L (21%), H-6→L (17%), H→L+1 (40%), H-14→L (3%), H-11→L (5%), H-4→L (2%), H-1→L+1 (3%)	0.00
$S_0 \rightarrow S_{15}$	313	3.94	H-12→L (96%)	0.00
$S_0 \rightarrow S_{16}$	312	3.96	H-14→L (44%), H-13→L (15%), H-11→L (18%), H-10→L (12%), H-12→L (2%), H→L+2 (2%)	0.00
$S_0 \rightarrow S_{17}$	307	4.03	H-14→L (15%), H-13→L (29%), H-2→L+1 (39%), H-3→L+1 (9%)	0.00
$S_0 \rightarrow S_{18}$	306	4.04	H-14→L (13%), H-13→L (33%), H-2→L+1 (41%), H-3→L+1 (3%), H-1→L+1 (2%)	0.00
$S_0 \rightarrow S_{19}$	303	4.08	H-15→L (69%), H-3→L+1 (14%), H-19→L (5%), H-2→L+1 (3%), H-1→L+1 (3%)	0.00
$S_0 \rightarrow S_{20}$	302	4.09	H-15→L (18%), H-3→L+1 (59%), H-17→L (3%), H-13→L (2%), H-2→L+1 (6%), H-1→L+1 (5%)	0.00

*H-HOMO, L-LUMO

CONCLUSIONS

In this study, we have investigated the thermodynamic parameters, adsorption energies and electronic properties of FUR and TIO into BNNT(6,6-8) using DFT/B3LYP calculations. The results show that the energy gaps of the complexes FUR/BNNT and TIO/BNNT are decreased rather than isolated BNNT(6,6-8). Therefore, the electrical conductivity of the complexes increase rather than the isolated BNNT(6,6-8). The reactivity of TIO is higher due to the lower η value (1.63 eV) rather than the FUR (1.65 eV). The complexes FUR/BNNT and TIO/BNNT have a high chemical activity, low chemical stability due to the decreasing electronic chemical potential (μ) and they are the soft systems rather than two azomethines and BNNT(6,6-8). NBO analysis predicted a charge transfer from the molecules FUR and TIO to BNNT(6,6-8) and from BNNT(6,6-8) to FUR and TIO. The encapsulation of the molecule FUR into the BNNT(6,6-8) enhances the value of λ_{max} (from 407 nm to 420 nm) and interaction of the TIO with the BNNT(6,6-8) increases the value of λ_{max} (from 409 nm to 423 nm), therefore they can be considered as a bathochromic shift. We hope that our results from the investigation of adsorption effects of two azomethines (FUR and TIO) with BN nanotube can be used as in the medicine chemistry as drug delivery system or in the field of environmental chemistry as an absorbent system in order to adsorption of the azomethine dyes.

REFRENCES

[1] Sheikhi, M., Shahab, S., Khaleghian, M., Kumar, R. (2018). Interaction between New Anti-cancer Drug Syndros and CNT (6,6-6) Nanotube for Medical Applications: Geometry Optimization, Molecular Structure, Spectroscopic (NMR, UV/Vis, Excited state), FMO, MEP and HOMO-LUMO Investigation. Appl. Surf. Sci., 434: 504–513.

[2] Sheikhi, M., Shahab, S., Filippovich, L., Khaleghian, M., Dikusar, E., Mashayekhi, M. (2017). Interaction between new synthesized derivative of (E,E)-azomethines and BN(6,6-7) nanotube for medical applications: Geometry optimization, molecular structure, spectroscopic (NMR, UV/Vis, excited state), FMO, MEP and HOMO-LUMO investigations. J. Mol. Struct., 1146: 881–888.

[3] Ashraf, M.A., Liu, Z., Najafi, M. (2020). DFT Study of CN Oxidation (CN + ½O2 → OCN) on the Surfaces of Chromium-Doped Nanotubes (Cr–CNT (8,0) and Cr–BNNT (8,0)). Russ. J. Phys. Chem. B, 14: 217–221.

[4] Mickelson, W., Aloni, S., Han, W.Q., Cumings, J., Zettl, A. (2003). Packing C60 in Boron Nitride Nanotubes. Science, 300, 467–469.

[5] Oku, T., Hirano, T., Kuno, M., Kusunose, T., Niihara, K., Suganuma, K. (2000). Synthesis, atomic structures and properties of carbon and boron ni-

tride fullerene materials. Mater. Sci. Eng. B, 74: 206–217.

[6] Oku, T., Hiraga, K., Matsuda, T., Hirai, T., Hirabayashi, M. (2003). Twin structures of rhombohedral and cubic boron nitride prepared by chemical vapor deposition method. Diamond Relat. Mater., 12: 1138–1142.

[7] Khaleghian, M., Azarakhshi, F. (2019). Theoretical modelling of encapsulation of the Altretamine drug into BN(9,9-5) and AlN(9,9-5) nano rings: a DFT study. Mol. Phys., 117: 2559–2569.

[8] Golberg, D., Bando, Y., Tang, C.C., Zhi, Adv. C.Y. (2007). Boron Nitride Nanotubes. Adv. Mater., 19: 2413–2432.

[9] Shahab, S., Sheikhi, M., Filippovich, L., Dikusar, E., Yahyaei, H., Kumar, R., Khaleghian, M. (2018). Design of geometry, synthesis, spectroscopic (FT-IR,UV/Vis, excited state, polarization) and anisotropy (thermal conductivity and electrical) properties of new synthesized derivatives of (E,E)- azomethines in colored stretched poly (vinyl alcohol) matrix. J. Mol. Struct., 1157: 536–550.

[10] Sheikhi, M., Shahab, S., Filippovich, L., Yahyaei, H., Dikusar, E., Khaleghian, M. (2018). New derivatives of (E,E)-azomethines: Design, quantum chemical modeling, spectroscopic (FT-IR, UV/Vis, polarization) studies, synthesis and their applications: Experimental and theoretical investigations. J. Mol. Struct., 1152: 368–385.

[11] Jarrahpour, A., Zarei, M. (2010). Efficient one-pot synthesis of 2-azetidinones from acetic acid derivatives and imines using methoxymethylene-N,N-dimethyliminium salt. Tetrahedron, 66: 5017–5023.

[12] Zhao, X., Li, C., Zeng, S., Hu, W. (2011). Discovery of highly potent agents against influenza A virus. Eur. J. Med. Chem., 46: 52–57.

[13] Almodarresiyeh, H., Shahab, S., Zelenkovsky, V., Ariko, N., Filippovich, L., Agabeko, V. (2014). Calculation of UV, IR, and NMR spectra of diethyl 2,20-[(1,10-Biphenyl)-4,40 diylbis(azanediyl)] diacetate. J. Appl. Spectrosc., 81: 31–36.

[14] Shahab, S., Kumar, R., Darroudi, M., Borzehandani, M.Y. (2015). Molecular structure and spectroscopic investigation of sodium(E)-2-hydroxy-5-((4-sulfonatophenyl) diazenyl)benzoate: a DFT study. J. Mol. Struct., 1083: 198–203.

[15] Iwan, A., Schab-Balcerzak, E., Grucela-Zajac, M., Skorka, L. (2014). Structural characterization, absorption and photoluminescence study of symmetrical azomethines with long aliphatic chains. J. Mol. Struct., 1058: 130–135.

[16] Iwan, A., Palewicz, M., Krompiec, M., Grucela-Zajac, M., Schab-Balcerzak, E., Sikora, A. (2012). Synthesis, Materials Characterization and Opto(electrical) Properties of Unsymmetrical Azomethines With Benzothiazole. Core. Mol. Biomol. Spectrosc, 97: 546–555.

[17] Nowak, E.M., Sanetra, J., Grucela, M., Schab-Balcerzak, E. (2015). Azomethine naphthalene diimides as component of active layers in bulk heterojunction solar cells. Mater. Lett., 157, 93–98.

[18] Feazell, R.P., Nakayama-Ratchford, N., Dai, H. Lippard, S. J. (2007). Soluble Single-Walled Carbon Nanotubes as Longboat Delivery Systems for Platinum(IV) Anticancer Drug Design. J. Am. Chem. Soc., 129: 8438–8439.

[19] Dhar, S., Liu, Z., Thomale, J., Dai, H., Lippard, S.J. (2008). Targeted Single-Wall Carbon Nanotube-Mediated Pt(IV) Prodrug Delivery Using Folate as a Homing Device. J. Am. Chem. Soc., 130: 11467–11476.

[20] Liu, Z., Chen, K., Davis, C., Sherlock, S., Cao, Q., Chen, X., Dai, H. (2008). Drug delivery with carbon nanotubes for in vivo cancer treatment. Cancer Res., 68: 6652–6660.

[21] Pastorin, G., Wu, W., Wieckowski, S., Briand, J.P., Kostarelos, K., Prato, M., Bianco, A. (2006). Double functionalisation of carbon nanotubes for multimodal drug delivery. Chem. Comm., 11: 1182–1184.

[22] Ali-Boucetta, H., Al-Jamal, K.T., McCarthy, D., Prato, M., Bianco, A., Kostarelos, K. (2008). Multiwalled carbon nanotube–doxorubicin supramolecular complexes for cancer therapeutics. Chem. Comm., 4: 459–461.

[23] Ajeel, F.N., Mohammed, M.H., Khudhair, A.M. (2019). SWCNT as a Model Nanosensor for Associated Petroleum Gas Molecules: Via DFT/B3LYP Investigations. Russ. J. Phys. Chem. B, 13: 196–204.

[24] Rezaei-Sameti, M., Pahlevane, M. (2017). A Computational Study of the Interaction CN− with the Pristine, Ge-Doped of AlPNTs. Russ. J. Phys. Chem. B, 11: 985–1001.

[25] Chen, Z., Shao, Z., Siddiqui, M.K., Nazeer, W., Najafi, M. (2019). Potential of Carbon, Silicon, Boron Nitride and Aluminum Phosphide Nanocages as Anodes of Lithium, Sodium and Potassium Ion Batteries: A DFT Study. Russ. J. Phys. Chem. B, 13, 156–164.

[26] Hassan, A.J. (2019). Hydrochlorofluorocarbons Adsorption on Undoped and Al-Doped Graphene Nanoflakes by Using Density Functional Theory (DFT) Study. Russ. J. Phys. Chem. B, 13: 1064–1069.

[27] Jayabharathi, J., Thanikachalam, V., Venkatesh Perumal, M., Srinivasan, N. (2011). A physiochemical study of azo dyes: DFT based ESIPT process. Spectrochimica Acta Part A, 83: 200– 206.

[28] Frisch, M.J., Trucks, G.W., Schlegel, H.B., Scuseria, G.E., Robb, M. A., Cheeseman, J.R., Scalmani, G., Barone, V., Mennucci, B., Petersson, G.A., Nakatsuji, H., Caricato, M., Li, X., Hratchian, H.P., Izmaylov, A.F., Bloino, J., Zheng, G., Sonnenberg, J.L., Hada, M., Ehara, M., Toyota, K., Fukuda, R., Hasegawa, J., Ishida, M., Nakajima, T., Honda, Y., Kitao, O., Nakai, H., Vreven, T., Montgomery, J.A., Peralta, J.E., Ogliaro, F., Bearpark, M., Heyd, J.J., Brothers, E., Kudin, K.N., Staroverov, V.N., Kobayashi, R., Normand, J., Raghavachari, K., Rendell, A., Burant, J.C., Iyengar, S.S., Tomasi, J., Cossi, M., Rega, N., Millam, J.M., Klene, M., Knox, J.E., Cross, J.B., Bakken, V., Adamo, C., Jaramillo, J., Gomperts, R., Stratmann, R.E., Yazyev, O., Austin, A.J., Cammi, R., Pomelli, C., Ochterski, J.W., Martin, R.L., Morokuma, K., Zakrzewski, V.G., Voth, G.A., Salvador, P., Dannenberg, J.J., Dapprich, S., Daniels, A.D., Farkas, Ö., Foresman, J.B., Ortiz, J.V., Cioslowski, J., Fox, D.J. (2009). Gaussian 09 revision A02, Gaussian, Inc., Wallingford CT.

[29] Sheikhi, M., Shahab, S., Khaleghian, M., Haji Hajikolaee, F., Balakhanava, I., Alnajjar, R. (2018). Adsorption Properties of the Molecule Resveratrol on CNT(8,0-10) Nanotube: Geometry Optimization, Molecular Structure, Spectroscopic (NMR, UV/Vis, Excited State), FMO, MEP and HOMO-LUMO Investigations. J. Mol. Struct., 1160: 479–487.

[30] Frisch, A., Nielsen, A.B., Holder, A. J. (2000). Gauss View Users Manual, Gaussian Inc.

[31] O'Boyle, N., Tenderholt, A., Langner. K. (2008). Cclib: a library for package-independent computational chemistry algorithms, J. Comput. Chem., 29: 839–845.

[32] Shahab, S., Sheikhi, M., Filippovich, L., Khaleghian, M., Dikusar, E., Yahyaei, H., Yousefzadeh Borzehandani, M. (2018).Spectroscopic Studies (Geometry Optimization,E→ZIsomerization,UV/Vis, Excited States, FT-IR, HOMO-LUMO, FMO, MEP, NBO,Polarization) and Anisotropy of Thermal and Electrical Conductivityof New Azomethine Dyes in Stretched Polymer Matrix. Silicon, 10: 2361–2385.

[33] Weinhold, F., Landis, C.R. (2001). Natural Bond Orbitals and Extensions of Localized. Res. Pract. Eur., 2: 91–104.

AUTHOR (S) BIOSKETCHES

Samireh Esmaeili, PhD, Department of Chemistry, Central Tehran Branch, Islamic Azad University, Tehran, Iran

Mehrnoosh Khaleghian, Assistant Professor, Department of Chemistry, Islamshahr Branch, Islamic Azad University, Islamshahr, Iran, *E-mail: mehr.khaleghian97@gmail.com*

Marjaneh Samadizadeh, Associate Professor, Department of Chemistry, Central Tehran Branch, Islamic Azad University, Tehran, Iran